Wave-packet dynamics of resonant x-ray Raman scattering: Excitation near the Cl $L_{II,III}$ edge of HCl

Paweł Sałek, Faris Gel'mukhanov,* and Hans Ågren
Institute of Physics and Measurement Technology, Linköping University, S-581 83 Linköping, Sweden
(Received 21 April 1998; revised manuscript received 9 September 1998)

A theory of radiative and nonradiative x-ray Raman scattering based on nuclear wave-packet dynamics is presented. The theory is evaluated with special emphasis on the cases when the intermediate and/or final state potentials are dissociative. Different ''one-step'' and ''two-step'' time-dependent wave-packet formalisms are proposed and evaluated, giving different interpretational content and computational efficiency. An interference between the molecular background and the narrow atomiclike contributions is predicted and evaluated. Due to this interference the atomiclike spectral feature manifests itself as a peak or as a spectral hole depending on the circumstances in terms of excitation energy, spectral width of incident radiation, and the form of the interatomic potentials. The counterintuitive situation may even arise that a narrow peak is formed by increasing the spectral photon width. The duration of the resonant x-ray Raman scattering influences in a qualitatively different manner the space distributions of the wave packets in the molecular and the dissociative domains, something that is crucial for the formation of the cross section profile. It is shown that the scattering cross section is proportional to the square of the core excited wave packet and inversely proportional to the derivative of the difference between core excited and final state potentials. The atomiclike profile is shown to consist of a Lorentzian inner part and red or blue wings which give direct information about the long-range regions of the potentials; red wings for diverging potentials, and blue for converging. A technique of mapping of the space distribution of the squared core excited wave packet and the interatomic potentials is suggested. The various features are demonstrated by an *ab initio* computational study of the resonant Auger spectra of the HCl molecule close to the Cl $L_{II,III}$ edge. [S1050-2947(99)04702-2]

PACS number(s): 33.20.Rm, 33.50.Dq, 33.70.−w

I. INTRODUCTION

At the present time rich experimental and theoretical material has been accumulated in the field of resonant x-ray Raman scattering for gas and condensed systems, covering a wide range of the x-ray wavelength region [1–8]. The development has taken turns in many directions and branches of investigations. One such branch comprises resonant x-ray scattering (RXS) of systems for which the coupling to the nuclear degrees of freedom is essential and for which the RXS profile and its excitation energy dependence also refer to the nuclear motion. Although the first fundamental results are a quarter century old for *nonresonant* x-ray emission and Auger spectra—like the discovery of the vibrational structure [9,10] and the lifetime-vibrational interference effects [11]—most of the results in the *resonant* case have been obtained only fairly recently [12,6,13,14]; a few examples to mention are the connection between vibrational structure and nonlinear dispersion [15–17], the collapse effect [18,19], and the effects of violation [20–23] and restoration of the selection rules [22,23].

A set of interesting observations has been presented for RXS under core excitation to dissociative states [24,25,8]. Perhaps the most striking one is that the RXS spectral profile consists of two qualitatively different parts; the so-called ''molecular'' and ''atomiclike'' parts [26,25,27–29], and that the relative cross sections for these two parts strongly depend on the frequency detuning, and therefore on the duration of the RXS process [26,18,27]. Other related spectral features are caused by the so-called electron Doppler effect for dissociative states [30].

The aim of this paper is to present a dynamical theory of RXS using wave packets, and to demonstrate this theory to an actual molecular system studied experimentally. The consequences of the theory are investigated in some detail for x-ray Raman scattering involving core excitations to dissociative states, especially the spectral features of the so-called atomic-like resonance and the ''molecular'' background. It is shown that the interference between these two contributions gives rise to new, and quite unexpected, effects. The mapping of the wave packet and the interatomic potentials is of further interest in that context [26].

The outline of the paper follows. After a short theoretical introduction in Sec. II, we formulate in Sec. III three qualitatively different time-dependent strategies (Secs. III A, III B, and III C) for the evaluation of the RXS cross section. In the beginning of Sec. IV we briefly outline approximations and some features of the time-dependent theory of RXS with nuclear degrees of freedom. The next Section (Sec. V) is devoted to the mapping of the core excited state wave packet and internuclear potentials. Our semiclassical analysis of this problem is based on Wigner's transform. The reflection techniques used for the mapping procedure qualitatively differ for the molecular (Secs. V A, V D) and dissociative (Secs. V B, V D) regions. The role of the excitation energy in the space distribution of the wave packet is investigated in Sec. V C. In Sec. V E we show that the atomiclike profile

*Permanent address: Institute of Automation and Electrometry, 630090 Novosibirsk, Russia.

consists of a Lorentzian plus short- or long-wavelength wings depending on the long-range part of the potentials. The interference of the molecular background and the atomiclike resonance and the spectral consequences of this interference are discussed in Sec. VI B. Section VII summarizes the paper.

II. THEORETICAL BACKGROUND

By absorbing an incoming x-ray photon with the frequency ω a molecule is core excited to the state $|c\rangle$. Due to the Coulomb interaction and vacuum fluctuations this intermediate core excited state decays by emitting Auger electrons and x-ray photons with the energy E to the final state $|f\rangle$.

The spectral properties of RXS are guided by the double differential cross section [1,31]

$$\sigma(E,\omega)=\sum_f |F|^2\Phi(\omega-E-\omega_{f0},\gamma), \tag{1}$$

which is the convolution of the spectral distribution Φ of the incident radiation with the RXS cross section $\sigma_0(E,\omega)$ for a monochromatic incident light beam. Here γ is the spectral width of Φ. In order to make the formal manipulations more transparent, we drop the index f in the scattering amplitude: $F_f \rightarrow F$. We focus only on the spectral shape of RXS, therefore the cross section is written here without the multiplication factor. The radiative and nonradiative RXS amplitudes have the same structure near the resonant region [1],

$$F=\sum_c \frac{\langle f|Q|c\rangle\langle c|\mathcal{D}|0\rangle}{E-\omega_{cf}+\imath\Gamma}. \tag{2}$$

Here $\omega_{cf}=E_c-E_f$, E_c is the energy of the cth state, and Γ is the lifetime broadening of the core excited state. The lifetime broadening of the final state Γ_f is often small and is neglected here for simplicity. The operator $\mathcal{D}$ describes the interaction of the target with the incident x-ray photon. In the case of nonradiative RXS, Q is the Coulomb operator, and $Q=\mathcal{D}'^*$ when the emitted particle is the final x-ray photon [1]. (Atomic units are used unless otherwise stated.)

III. TIME-DEPENDENT REPRESENTATION FOR THE RXS CROSS SECTION

The half Fourier transform of the denominator on the right-hand side of Eq. (2) yields the time-dependent representation for the scattering amplitude [32,26]

$$F=F(\infty), \quad F(\tau)=-\imath\int_0^\tau dt\, e^{\imath(E+E_f+\imath\Gamma)t}\langle f|\phi(t)\rangle. \tag{3}$$

The wave packet reads

$$|\phi(t)\rangle=Qe^{-\imath H_c t}\mathcal{D}|0\rangle. \tag{4}$$

Let us note that in strict theory the molecular Hamiltonian H is the same for all electronic states j (except final state in nonradiative RXS). However, we will use notation H_j with index j due to two reasons; first to identify the electronic shell in which the wave packet evolves, and, secondly, to apply directly the general theory to nuclear degrees of freedom with the nuclear Hamiltonian depending on the electronic state j. A corresponding time-dependent representation for the RXS cross section (1) can be obtained by a Fourier transform of the spectral function $\Phi(\omega,\gamma)$,

$$\Phi(\omega,\gamma)=\frac{1}{\pi}\mathrm{Re}\int_0^\infty dt\,\varphi(t,\gamma)e^{\imath\omega t},$$

$$\varphi(t,\gamma)=\int_{-\infty}^\infty d\omega\,\Phi(\omega,\gamma)e^{-\imath\omega t}. \tag{5}$$

Since the function $\Phi(\omega,\gamma)$ is real, its Fourier transform has the property $\varphi^*(t,\gamma)=\varphi(-t,\gamma)$. We note that $\varphi(t,\gamma)=\delta(t)$ and $\varphi(t,\gamma)=\text{const}$ correspond to the cases of having white and monochromatic incident light beams, respectively. Very often the spectral function Φ is approximated by a Gaussian. In this case the following formulas are useful:

$$\Phi(\omega,\gamma)=\frac{1}{\gamma\sqrt{\pi}}\exp\left(-\frac{\omega^2}{\gamma^2}\right), \quad \varphi(t,\gamma)=\exp\left(-\frac{t^2\gamma^2}{2}\right). \tag{6}$$

To receive the time-dependent representation for the RXS cross section we follow the method outlined in Refs. [11, 26]. Substituting Eqs. (3) and (5) in Eq. (1) the following dynamical representation for the RXS cross section is obtained:

$$\sigma(E,\omega)=\frac{1}{\pi}\mathrm{Re}\int_0^\infty d\tau\,\sigma(\tau)\varphi(\tau,\gamma)e^{\imath(\omega-E+E_0)\tau} \tag{7}$$

in terms of the autocorrelation function

$$\sigma(\tau)=\langle\psi_E(0)|\psi_E(\tau)\rangle. \tag{8}$$

Here

$$|\psi_E(\tau)\rangle=e^{-\imath H_f\tau}|\psi_E(0)\rangle, \quad |\psi_E(0)\rangle=\int_0^\infty dt\,e^{(\imath E-\Gamma)t}|\psi(t)\rangle. \tag{9}$$

The wave packet $|\psi_E(\tau)\rangle$ with the initial value $|\psi_E(0)\rangle$ is the solution of the nonstationary Schrödinger equation with the final state Hamiltonian H_f, whereas the wave packet

$$|\psi(t)\rangle=e^{\imath H_f t}Qe^{-\imath H_c t}\mathcal{D}|0\rangle \tag{10}$$

admits two different interpretations and computational strategies.

A. Two-step evolution of the wave packet

The two-propagator representation (10) prompts that

$$|\psi(t)\rangle=|\psi(0,t)\rangle, \quad |\psi(\tau,t)\rangle=e^{iH_f(t-\tau)}Qe^{-iH_c t}\mathcal{D}|0\rangle \tag{11}$$

is the result of a two-step evolution: The initial wave packet $\mathcal{D}|0\rangle$ after core excitation propagates in the core excited state from time equal to 0 up to t. Then after the decay transition at moment t the wave packet evolves in the final state in the

opposite time direction from moment t up to 0. The evolution of the wave packet $|\psi(\tau,t)\rangle$ is given by two coupled Schrödinger equations

$$i\frac{\partial}{\partial\tau}|\psi(\tau,t)\rangle=H_f|\psi(\tau,t)\rangle,\quad |\psi(t,t)\rangle=Q|\psi_c(t)\rangle,$$
$$i\frac{\partial}{\partial t}|\psi_c(t)\rangle=H_c|\psi_c(t)\rangle,\quad |\psi_c(0)\rangle=\mathcal{D}|0\rangle. \tag{12}$$

B. One-step dynamics

A conceptually different interpretation of the wave packet (10) is based on the one-step dynamics with one effective time-dependent Hamiltonian $\Delta V(t)$. By differentiation of Eq. (10) with respect to t we obtain the following Schrödinger equation:

$$i\frac{\partial}{\partial t}|\psi(t)\rangle=\Delta V(t)|\psi(t)\rangle,\quad \Delta V(t)=e^{iH_ft}\Delta V e^{-iH_ft},$$
$$\Delta V=QH_cQ^{-1}-H_f, \tag{13}$$

with the initial condition $|\psi(0)\rangle=Q\mathcal{D}|0\rangle$. The solution of the latter equation is straightforward,

$$|\psi(t)\rangle=\mathcal{U}(t,t_0)|\psi(t_0)\rangle,$$
$$\mathcal{U}(t,t_0)=T\exp\left(-\imath\int_{t_0}^{t}dt_1\Delta V(t_1)\right), \tag{14}$$

where T is the time-ordering operator.

At this point it is worth pointing out the following striking property of the wave packet $|\psi(t)\rangle$: The evolution of $|\psi(t)\rangle$ is completely halted in the dissociative region where $\Delta V\rightarrow\omega_{cf}(\infty)\equiv U_c(\infty)-U_f(\infty)$ since the evolution operator $\mathcal{U}(t,t_0)$ (14) then becomes equal to the c-number:

$$\Delta U(R)\simeq\omega_{cf}(\infty),\quad \mathcal{U}(t,0)\simeq e^{-i\omega_{cf}(\infty)t},$$
$$|\psi(t)\rangle\simeq e^{-i\omega_{cf}(\infty)t}|0\rangle. \tag{15}$$

The same result follows immediately also from the two-step representation (10), since in the dissociative region $H_c\simeq H_f+\omega_{cf}(\infty)$ and hence again $|\psi(t)\rangle\simeq\exp[-\imath\omega_{cf}(\infty)t]|0\rangle$. This result is important also from the viewpoint of numerical simulations since it makes it possible to avoid the integration of Eq. (13) as well as of Eqs. (12) in the region of dissociation.

The two-step and one-step approaches for the evaluation of the wave packet $|\psi(t)\rangle$ (10) lead to two qualitatively different numerical techniques. The two-step technique requires more computational time because the solution of the time-dependent Schrödinger equation (12) for $|\psi(\tau,t)\rangle$ requires in advance the solution of the time-dependent Schrödinger equation for $|\psi_c(t)\rangle$. The one-step method is free from this disadvantage, but contains on the other hand the complicated operator $\Delta V(t)$ which needs to be diagonalized.

We propose also a third method for a time-dependent evaluation of the RXS cross section, namely, one which is based on the evolution of the RXS cross section for monochromatic excitation with the forthcoming convolution of this cross section with the spectral function. This version will be preferred over the one- and two-step techniques.

C. Convolution of the cross section for narrow-band excitation

The main characteristic features of RXS can be seen when the spectral width γ of the incident light beam is small. The spectral function $\Phi(\omega,\gamma)$ for the narrow-band incident beam ($\gamma\ll\Gamma$) can be replaced in Eq. (1) by the Dirac δ function. Hence, the denominator in Eq. (1) becomes equal to $[\omega-(E_c-E_0)+\imath\Gamma]$. The autocorrelation function takes the form

$$\sigma(\tau)\rightarrow\sigma_0(\tau)=\langle\Psi(0)|\Psi(\tau)\rangle. \tag{16}$$

Here

$$|\Psi(\tau)\rangle=e^{-iH_f\tau}|\Psi(0)\rangle,$$
$$|\Psi(0)\rangle=\int_0^\infty dt\,e^{[i(\omega+E_0)-\Gamma]t}Q|\psi_c(t)\rangle. \tag{17}$$

We again obtain a two-step technique; (1) the solution of the Schrödinger equation (12) for $|\psi_c(t)\rangle=\exp(-iH_ct)\mathcal{D}|0\rangle$ with the initial condition $|\psi_c(0)\rangle=\mathcal{D}|0\rangle$, and (2) the solution of the Schrödinger equation for $|\Psi(t)\rangle$ with the final state Hamiltonian H_f and with the initial condition $|\Psi(0)\rangle$. However, this two-step technique has a big advantage over the first one mentioned above, since the initial condition $|\Psi(0)\rangle$ does not depend on time.

Having settled the question of evaluation of the RXS cross section $\sigma_0(E,\omega)$ for the monochromatic incident x-ray beam, we can evaluate the RXS cross section $\sigma(E,\omega)$ (1) for arbitrary spectral distribution of incoming radiation as the following convolution [31]:

$$\sigma(E,\omega)=\int d\omega_1\sigma_0(E,\omega_1)\Phi(\omega-\omega_1,\gamma),$$
$$\sigma_0(E,\omega)=\frac{1}{\pi}\mathrm{Re}\int_0^\infty d\tau\,\sigma_0(\tau)e^{i(\omega-E+E_0)\tau}. \tag{18}$$

From the computational point of view the method given by these equations is both simpler and faster in comparison with the two techniques described above (see Secs. III A and III B).

Another computational advantage of this approach is the inherent parallelism: The cross sections $\sigma_0(E,\omega)$ are independent of each other and their evaluation can therefore be performed on a parallel machine with ease. The only serial operations in the program are the generation of the initial condition $|0\rangle$ and the the final convolution (18) and they consume much less time than the evaluation of $\sigma_0(E,\omega)$. The scheme was implemented and the parallel efficiency that was above 95% and that did not depend on the number of nodes used.

IV. NUCLEAR DYNAMICS

We now turn to the important special case in RXS when only the nuclear degrees of freedom can be taken into account, which often can be motivated when the different elec-

tronic transitions in the RXS spectra are well separated. RXS experiments show strong dependences of the spectral profile on the nuclear motion and the vibrational degrees of freedom. This means vibrational structure in the case of bound-bound-bound transitions [3,5,6,14] and the interplay of the so-called molecular and atomiclike contributions to the spectrum when the molecule is core excited above the dissociation threshold [26,27]. Let us assume here the validity of the Born-Oppenheimer (BO) approximation which allows the separation of the nuclear and electronic degrees of freedom. We will also neglect the dependence of the electronic transition matrix elements D and Q on the nuclear coordinates. This approximation is sufficiently good for the photoabsorption matrix element D since the ground state nuclear wave function is localized close to the equilibrium molecular geometry. The same assumption concerning the amplitude of the decay transition Q can be justified for the bound-bound decay transitions. However, this dependence of Q can be more essential for the continuum-continuum decay transitions since a large span of internuclear distances then is involved, and this dependence might influence the ratio of the molecular and atomiclike contributions. On the other hand, for hydrides with one heavy atom, like HCl, the total rate is probably dominated by the heavy atom. Investigations of the partial and the total Auger decay rate for the H_2O molecule indeed indicate that most of the internuclear dependence of these rates is allocated at distances shorter than the equilibrium, and that the ''constant resonance width'' approximation holds [33].

When the R dependence of the transition matrix elements is weak, D and Q can be factored out, and thus one can simplify the RXS amplitude by setting

$$\mathcal{D}=Q=1. \tag{19}$$

[Notice that we will use approximation $\mathcal{D}=\text{const}$, $Q=\text{const}$ only in our numerical simulations and in the expressions for the Franck-Condon (FC) factors. All other results are free from this assumption.] The question of interest is posed by the pure nuclear problem with the Hamiltonians

$$H_\alpha=K+U_\alpha(R), \quad \alpha=0,c,f. \tag{20}$$

Here K is the nuclear kinetic energy operator.

It is relevant to note the physical meaning of the wave packet $|\psi(t)\rangle$ (10) in the $Q=\text{const}$ approximation. The one-step (13) evolution of this wave packet is given exactly by the interaction picture with H_f as the unperturbed Hamiltonian and

$$\Delta V=\Delta U(R) \tag{21}$$

as the perturbation. One obtains the remarkable result that the one-step dynamics is determined by the difference $\Delta U(R)$ between potentials of the core exited $U_c(R)$ and final $U_f(R)$ states.

V. MAPPING OF THE CORE EXCITED WAVE PACKETS AND POTENTIALS. THE REFLECTION TECHNIQUE

Another physical interpretation of the wave packet $|\Psi(0)\rangle$ is obtained by first considering RXS with a monochromatic incident x-ray beam. In this case the RXS amplitude (2) becomes the projection of the coherent superposition of the core excited states $|\Psi(0)\rangle$ on the final state

$$F_f=-i\langle f|\Psi(0)\rangle, \quad |\Psi(0)\rangle=i\sum_c \frac{Q|c\rangle\langle c|\mathcal{D}|0\rangle}{\omega-\omega_{c0}+i\Gamma}. \tag{22}$$

This representation immediately shows that $|\Psi(0)\rangle$ (17) is the coherent superposition or ''wave train'' of the eigenstates of the core excited Hamiltonian H_c created due to the core excitation.

The ground is now prepared for expressing an entirely different representation for the RXS cross section (1),

$$\sigma_0(E,\omega)=\langle\Psi(0)|\,\delta(\mathcal{E}-H_f)|\Psi(0)\rangle=\text{tr}\,\delta(\mathcal{E}-H_f)\rho,$$
$$\rho=|\Psi(0)\rangle\langle\Psi(0)|, \tag{23}$$

with $\mathcal{E}=\omega+E_0-E$. We use also $\Psi(R,0)=\langle R|\Psi(0)\rangle$ for the coordinate representation of the wave packet $|\Psi(0)\rangle$.

Through this expression a mapping of the squared wave packet $\|\Psi(0)\rangle|^2$ and internuclear potentials can be obtained.

The easiest path to the desired semiclassical result is the Wigner transform (see Appendix A)

$$A_w(p,R)=\int dr\left\langle R+\frac{r}{2}\middle|A\middle|R-\frac{r}{2}\right\rangle e^{-ipr/\hbar}, \tag{24}$$

which gives a systematic procedure of an expansion in powers of $\hbar$. (Here we temporarily introduced Planck's constant since it is a key quantity in this expansion.)

We may write the semiclassical version of Eqs. (23) using the ansatz (A1) as

$$\sigma(E,\omega)\simeq\frac{1}{2\pi\hbar}\int dp\,dR\,\delta(\mathcal{E}-H_f(p,R))\rho_w(p,R), \tag{25}$$

with $H_f(p,R)=p^2/2\mu+U_f(R)$ as the classical Hamilton function and μ as the reduced mass of the molecule. This equation becomes

$$\sigma(E,\omega)\simeq\frac{\mu}{2\pi\hbar}\int\frac{dR}{p_0(R)}\rho_w(p_0(R),R),$$
$$p_0(R)=\{2\mu[\mathcal{E}-U_f(R)]\}^{1/2}. \tag{26}$$

To proceed further we use the conventional separation of the internuclear domain into two regions, the ''molecular'' ($R<R_d$) and the ''dissociative'' ($R>R_d$) regions. Here R_d is the minimal internuclear distance where $U_c(R)$ and $U_f(R)$ are close to the corresponding dissociation limits. Using this partitioning the RXS cross section (25) becomes the sum of the ''molecular'' and ''atomiclike'' contributions,

$$\sigma(E,\omega)=\sigma_{\text{mol}}(E,\omega)+\sigma_{\text{at}}(E,\omega), \tag{27}$$

which are defined by Eq. (25) with $\int_0^{R_d}dR$ and $\int_{R_d}^{\infty}dR$, respectively.

A. "Molecular" region: $R<R_d$

The molecular background is formed mainly by core excitation in the vicinity of the classical turning point $R=R_0$ where $p=0$ and, hence, the total nuclear energy is $U_c(R_0)$. More precisely, the core excitation close to $U_c(R_0)$ takes place at the band with the width $\gamma_c=a|U'(R_0)|$ of the photoabsorption FC factor $\langle\epsilon_c|0\rangle$ [26]. Here $a=1/\sqrt{\mu\omega_0}$ and ω_0 is the ground state vibrational frequency.

It is a good approximation to consider R_0 as the ground state internuclear distance. According to the energy conservation law the kinetic $\epsilon_c(R)$ and potential $U_c(R)$ energies satisfy the equation $U_c(R_0)=H_c(p,R)\equiv\epsilon_c(R)+U_c(R)$ at the arbitrary point R. This allows a replacement in Eq. (25) of the δ function by $\delta(E+\epsilon_f(R)+U_f(R)-\Omega-\epsilon_c(R)-U_c(R))$. Here we introduced the detuning of the excitation frequency

$$\Omega=\omega-\omega_{c0},\quad \omega_{c0}=U_c(R_0)-E_0 \tag{28}$$

relative to the resonant frequency of the "vertical" photoabsorption transition ω_{c0}. Recall that the molecular region corresponds to fast RXS. This means that the important points for the decay transition are those at which both R and p, and hence the kinetic energy, remain unaltered:

$$\epsilon_f(R)=\epsilon_c(R). \tag{29}$$

It is not difficult to see from Eq. (25) that

$$\sigma_{\rm mol}(E,\omega)\simeq\int_0^{R_d}dR\;\delta(E-\Omega-\Delta U(R))|\Psi(R,0)|^2,$$

$$\Delta U(R)=U_c(R)-U_f(R). \tag{30}$$

Here we used the important property of Wigner's function given by Eq. (A4).

B. Dissociation domain: $R>R_d$

Another spectral feature of the RXS profile is the atomiclike resonance which is formed primarily due to the decay transitions in the dissociation region. The formal origin of the atomiclike resonance is the Lorentzian in Eq. (2) with the resonance condition: $\omega+E_0=H_c(p,R)=\epsilon_c(R)+U_c(R)$. In the dissociative region the potentials are approximately constant in R; $U_c(R)\simeq$const, $U_f(R)\simeq$const. Therefore wave functions of both core excited and final nuclear states are close to plane wave solutions. This immediately leads to the conservation of kinetic energy under the decay transition (29). Similar to Eq. (30) this allows us to express

$$\sigma_{\rm at}(E,\omega)\simeq\int_{R_d}^{\infty}dR\;\delta(E-\Delta U(R))|\Psi(R,0)|^2. \tag{31}$$

Both Eqs. (30) and (31) constitute the reflection principle which allows us to map the squared wave packet $|\Psi(R,0)|^2$ for the different excitation energies.

One can easily identify a qualitative distinction between Eqs. (30) and (31); contrary to the case in the dissociative region (31) the reflection procedure $E=\Omega+\Delta U(R)$, Eq. (30) depends in the molecular region linearly on the detuning Ω. This results in the Raman dispersion law for the center of gravity of the molecular contribution. Clearly, the position of an atomiclike resonance (31) does not depend on the excitation energy.

As far as Eq. (30) is based on the assumption of a narrow FC factor $\langle\epsilon_c|0\rangle$, the Raman dispersion law $[E=\Omega+\Delta U(R)]$ for the molecular contribution is valid only in the region $(\Omega^2+\Gamma^2)^{1/2}>\gamma_c$. One can expect a breakdown of the linear dispersion law if ω is tuned inside of the region of the strong photoabsorption, $|\Omega|<\gamma_c$ [15].

C. Wave packets and space properties

Let us here consider some important features of the wave packet $|\Psi(0)\rangle$. Equations (B1) and (B4) show directly that the wave packet $\Psi(R,0)=\langle R|\Psi(0)\rangle$ in the dissociative region $R>R_d$ is a fast oscillating damped plane wave

$$\Psi(R,0)\simeq e^{\imath(R-R_d)p-\Gamma\tau_f}\Psi(R_d,0)\propto e^{\imath(R-R_d)p-\Gamma\tau_f}\times\exp\left[-\frac{1}{2}\left(\frac{\Omega}{\gamma_c}\right)^2\right],\quad R>R_d. \tag{32}$$

The time of flight in the dissociative region (B4) is merely $\tau_f\simeq(R-R_d)/v$, $v=p(\infty)/\mu$. The latter equation results immediately in an important consequence; the absolute value of the wave packet is a smooth function of R,

$$|\Psi(R,0)|\simeq e^{-\Gamma(R-R_d)/v}|\Psi(R_d,0)|. \tag{33}$$

An entirely different picture emerges in the molecular region $R<R_d$ where the momentum $p(R)$ strongly depends on R. Due to this dependence the wave packet (B1) is best expressed as a superposition, a "wave train," of many elementary waves [see Eqs. (22) and (B5)]. Obviously, the interference of these elementary waves leads to a smoother dependence of $\Psi(R,0)$ on R. An indirect confirmation of this fact is obtained at the limit of fast RXS (large RXS duration $1/\sqrt{\Omega^2+\Gamma^2}$) [26,18]. When the RXS is fast the decay transition thus occurs at the same point as the photoabsorption point

$$G(R,R')\simeq\frac{\delta(R-R')}{\Omega+\imath\Gamma}. \tag{34}$$

Hence the wave packet $\Psi(R,0)$ copies the space distribution of the ground state nuclear wave function $|0\rangle\equiv\varphi_0(R)$

$$\Psi(R,0)\simeq\imath\frac{\varphi_0(R)}{\Omega+\imath\Gamma}. \tag{35}$$

This equation can be used as a good estimation of the molecular contribution to the total RXS spectrum.

Let us briefly summarize the excitation energy dependence of the space distribution of $\Psi(R,0)$, Fig. 1. The so-called "molecular part" of the wave packet $(R<R_d)$ is a much smoother function of R than the long-distance contribution and decreases as $1/(\Omega+\imath\Gamma)$, Eq. (35), in the far wings of the photoabsorption band, $|\Omega|\gg\gamma_c$. This part of the wave packet is responsible for the formation of the molecular contribution $\sigma_{\rm mol}(E,\omega)$ or the far wings of the atomiclike resonance (Fig. 2). It is natural to refer to the part of $\Psi(R,0)$ lying in the dissociative region $R>R_0$ as the atom-

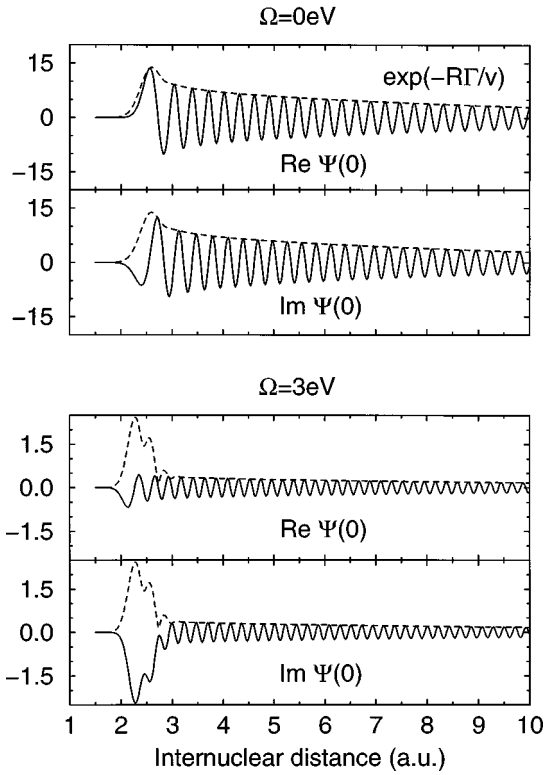

FIG. 1. Space distributions of the wave packet (17) in the dissociative core excited state ($2p^{-1}\sigma^*$) of HCl for different excitation energies ($\Omega=0$ and 3 eV). $\mathrm{Re}\,\Psi(R,0)$ and $\mathrm{Im}\,\Psi(R,0)$ are depicted as solid lines, while the absolute value $|\Psi(R,0)|$ of the wave packet is shown as a dashed line.

iclike part since the atomiclike resonance is formed in this region. The atomiclike part of $\Psi(R,0)$ demonstrates fast oscillations (32) with an exponential envelope (33) (Fig. 1). Notice that the absolute value $|\Psi(R,0)|$ is again a smooth function in the dissociative region, Fig. 1. Contrary to the molecular contribution the atomiclike part quenches faster, as $\exp[-(\Omega/\gamma_c)^2/2]$, when the absolute value of the detuning increases (see Fig. 1). This means that the molecule has no time to reach the dissociative region during the short RXS duration time $1/\sqrt{\Omega^2+\Gamma^2}$ [26]. The qualitative properties of the wave packet $|\Omega(0)\rangle$ described above are in excellent agreement with the results of the *ab initio* simulations presented in Fig. 1.

D. Mapping of the potentials and the squared wave packet

The general reflection technique described above contains an important special case which allows us to map $\Delta U(R)=U_c(R)-U_f(R)$. When the slope $\Delta U'(R)=d\Delta U(R)/dR$ is not equal to zero one can write

$$\sigma(E,\omega)\simeq\frac{\||\Psi(0)\rangle|^2}{|\Delta U'(R)|},\quad \Delta U(R)=\begin{cases}E-\Omega & \text{if } R<R_d\\ E & \text{if } R>R_d,\end{cases} \tag{36}$$

where the prime denotes a derivative with respect to position. What strikes the eye here is the simple relation between the RXS cross section and the slope $\Delta U'(R)$. This is important in the inverse problem of finding potentials from the spectroscopic measurements. However, the simplicity is

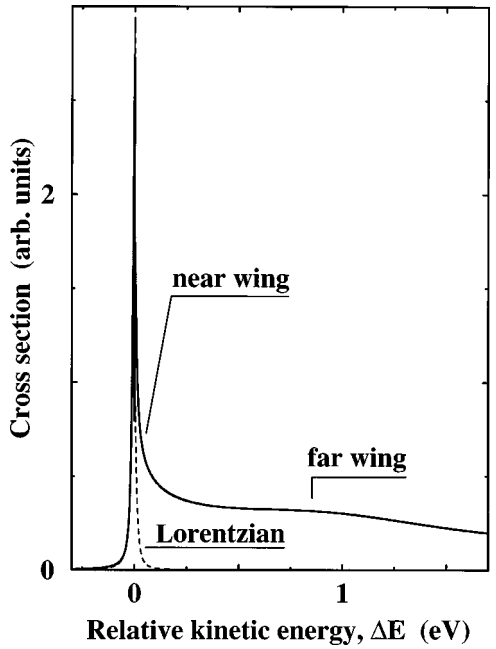

FIG. 2. Conventional partition of the spectral domain in the central (Lorentzian) part, near and far wings. $\Delta E=E-[U_c(\infty)-U_f(\infty)]$.

ephemeral in the molecular region where the wave packet $|\Psi(0)\rangle$ is a complicated function of R. The situation is more promising in the dissociative region where the R dependence of $|\Psi(R,0)|$,

$$|\Psi(R,0)|^2\simeq|\Psi(R_d,0)|^2e^{-2\tau_f/\tau},\quad \tau=\frac{1}{\Gamma} \tag{37}$$

is caused [26] only by the time of flight

$$\tau_f=\int^R\frac{dR}{v(R)}\simeq\frac{R}{v},$$

$$v(R)=\left(\frac{2}{\mu}[U_c(R_0)-U_c(R)]\right)^{1/2},\quad v=v(\infty). \tag{38}$$

and by the lifetime $\tau=1/\Gamma$. Though $|\Psi(R,0)|$ is a smooth function of R, $\Psi(R,0)$ shows the fast oscillations typical for the continuum states (Fig. 1). The atomiclike resonance and the corresponding near wing can dominate only when $\Omega=0$ [26,27,29]. Therefore to find $\Delta U(R)$ it is natural to tune ω in exact resonance, $\Omega=0$. Apparently, the reflection method maps the long-range part of $\Delta U(R)$ on the nearest wings of the atomiclike profile since the dependence of the potentials on R slow in the dissociative region (see Sec. V E).

The extension of the reflection technique to the whole spectral region allows us to map the ratio $|\Psi(R,0)|^2/|\Delta U'(R)|$, Eq. (36). This gives information about the space distribution of the squared wave packet (see Fig. 3). The comparison of the exact cross section with the one obtained in the reflection approximation indicates that the semiclassical approximation (36) is not perfect. The deviation with the exact cross section is stronger in the vicinity of the atomiclike resonance where the factor $1/|\Delta U'(R)|$ diverges and the semiclassical approximation breaks down.

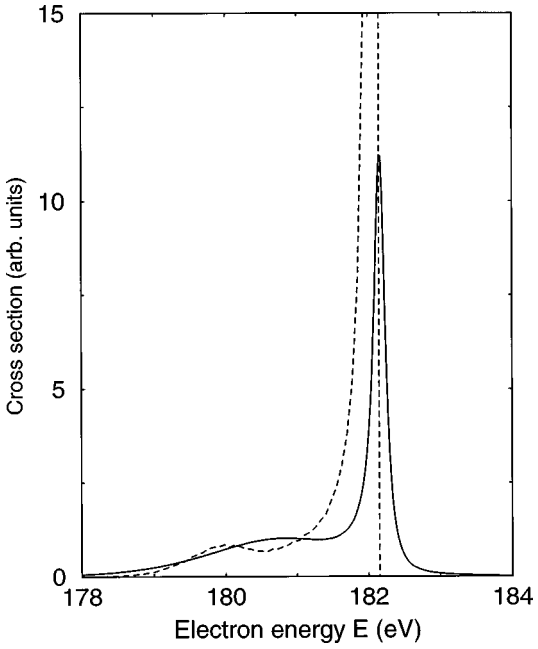

FIG. 3. Mapping of the ratio $|\Psi(R,0)|^2/|U'(R)|$ (36) (dashed line). The strict cross section of RXS in HCl is depicted by a solid line. The final state is $^4\Pi$. $\Omega=0$ eV.

E. Spectroscopy of the near wing of the atomiclike resonance

The atomiclike resonance is mainly formed by the spectral transition in one of the fragments of dissociation. If the central part of the atomiclike resonance line is close to a Lorentzian, the wings (the outer part) of the line have a different profile [26,27]. We are now prepared to describe the ''near wings'' (Fig. 2) more explicitly. To reduce the molecular contribution let us consider the case with $\Omega=0$. We are primarily interested in the dissociative region where the long-range forces dominate. Let us approximate here the difference $\Delta U(R)$ (31) of the core excited and final state potentials as

$$\Delta U(R)=\omega_{cf}(\infty)+\alpha\left(\frac{R_d}{R}\right)^n, \quad \omega_{cf}(\infty)=U_c(\infty)-U_f(\infty). \tag{39}$$

The solution of Eq. (36), $E=\Delta U(R)$, is straightforward: $R/R_d=[\alpha/(E-\Delta U(\infty)]^{1/n}$. The final results follow directly from Eqs. (31) and (37),

$$\sigma_{\rm at}(E,\omega)\simeq\sigma_0\left|\frac{\Delta}{\Delta E}\right|^{1+1/n}\exp\left(-\left|\frac{\Delta}{\Delta E}\right|^{1/n}\right),$$

$$\Delta E=E-\omega_{cf}(\infty), \tag{40}$$

where $\sigma_0=|\Psi(R_d,0)|^2[\tau/(2\tau_f^d)]^{n+1}R_d/(|\alpha|n)$, $\tau_f^d=R_d/v$, $\Delta=\alpha(2\tau_f^d/\tau)^n$.

The interpretation of this formula in the vicinity of the atomiclike resonance might lead to the wrong conclusion that $\sigma(E,\omega)\to 0$ when E tends to the resonant frequency of the atomiclike resonance $\omega_{cf}(\infty)$. This means that Eq. (40), as well as the reflection method based on Eqs. (31) and (36), describe only the wings of the atomiclike resonance. The formal reason of this limitation is that the asymptotical expansion of the RXS cross section in powers of $\hbar$ [based on Eq. (A2)] diverges as we approach the resonant frequency $\omega_{cf}(\infty)$ $(R\to\infty)$. One can show [for the power potentials (39)] that the ratio $\Delta\sigma_{\rm at}(E,\omega)/\sigma_{\rm at}(E,\omega)$ of the quantum correction $\Delta\sigma_{\rm at}(E,\omega)$ to the cross section (40) diverges as $|\Delta/\Delta E|^{1+1/n}$ when $\Delta E/\Delta\to 0$. The result is that the criterion of validity for the semiclassical expansion and, hence for Eq. (40), is $|\Delta E|\gg\Delta$. Hence, the red or blue wings of the atomiclike resonance are described by Eq. (36) and in the case of the power potential (39) as

$$\sigma_{\rm at}(E,\omega)\simeq\sigma_0\left|\frac{\Delta}{\Delta E}\right|^{1+1/n}. \tag{41}$$

However, we know that the spectral shape of the atomiclike resonance in the vicinity of the resonant frequency $\omega_{cf}(\infty)$ [26,25,27] is a Lorentzian

$$\sigma_{\rm at}(E,\omega)\propto\frac{\exp[-(\Delta E-\Omega)^2/\gamma_c^2]}{\Delta E^2+\Gamma^2}, \quad |\Delta E|<|\Delta|, \tag{42}$$

since in the soft x-ray region we commonly have that $\gamma_c\gg\Gamma$. To conclude, we point out that the spectral shape of the atomiclike resonance is the superposition of the Lorentzian (42) and the near wing [Eqs. (31), (36), and (40)] (Figs. 2 and 3).

The formula (40) involves the ratio $\Delta/\Delta E\propto\alpha/\Delta E$, which is positive. Indeed, the wing appears on the high-energy side of the atomiclike peak ($\Delta E>0$, Fig. 2) when the potentials of core excited and final states converge, $\Delta U(R)>\Delta U(\infty)$ $(\alpha>0)$, and vice versa, since $E=\Delta U(R)$. This yields the important consequence that the atomiclike resonance (42) has red or blue wings (40) if the potentials diverge $(\alpha>0)$ or converge $(\alpha<0)$, respectively, when $R\to\infty$ (see Sec. VI A).

VI. NUMERICAL APPLICATIONS: THE HCl MOLECULE

A. The RXS spectral shape versus potential surfaces and excitation energy

The experimental Auger spectrum [27] of HCl shows three peaks *A,B,C* lying near $E\approx 177.3$, 179.4, and 180.7 eV, respectively. We focus here mainly on the spectral region close to the *B* and *C* peaks. The following final molecular states of the HCl^+ ion correspond to these atomiclike lines: *B*: $^2\Pi$, $^2\Sigma^+$ and *C*: $^4\Pi$, $^2\Sigma^-$, $^4\Sigma^-$, $^2\Pi$. To understand the main spectral features of the resonant Auger electron decay spectra of the HCl molecule for the $2p^{-1}\sigma^*$ core excited state we accounted here for the three most important final states; the bound $^2\Sigma^+$ and the dissociative $^2\Sigma^-$ and $^4\Pi$ states. The corresponding potential surfaces (Fig. 4) have been calculated by the multiconfiguration self-consistent-field (MCSCF) method using the program DALTON [34].

Due to the spin-orbit splitting the core excited state $2p_{1/2}^{-1}\sigma^*$ is situated $\approx$1.67 eV higher than the $2p_{3/2}^{-1}\sigma^*$ state. The present calculations involves one (the lowest one) core excited state, $2p_{1/2,3/2}^{-1}\sigma^*$. The comparison with experiment becomes complicated when the detuning from the $2p_{3/2}^{-1}\sigma^*$ photoabsorption resonance is positive and core excitation of the $2p_{1/2}^{-1}\sigma^*$ also gets important. The evaluation of the electron matrix elements of the decay transitions Q is also outside the scope of the present paper. This means that the RXS

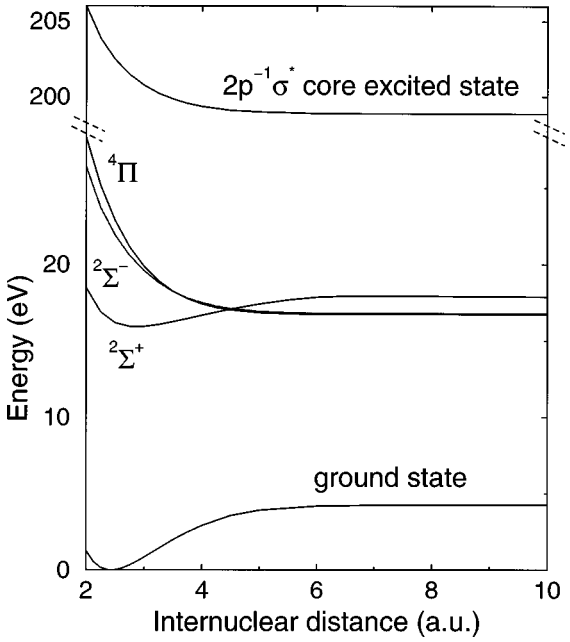

FIG. 4. Potential surfaces for ground, core excited ($2p^{-1}\sigma^*$), and final ($^4\Pi$, $^2\Sigma^-$, $^2\Sigma^+$) states of the HCl molecule.

cross section for different final states are given here for the same value of Q.

Figure 5 shows the RXS profiles for different final states for $\Omega=0$. One can see that the molecular bands can start from both the short-wave ($^2\Sigma^+$) and the long-wave ($^2\Sigma^-$,$^4\Pi$) sides of the atomiclike resonance. As was clarified above, blue and red tails are formed if the potential surfaces of the core excited and final states converge or diverge, respectively, when R increases and approaches the dissociation region. The atomiclike resonance for the same

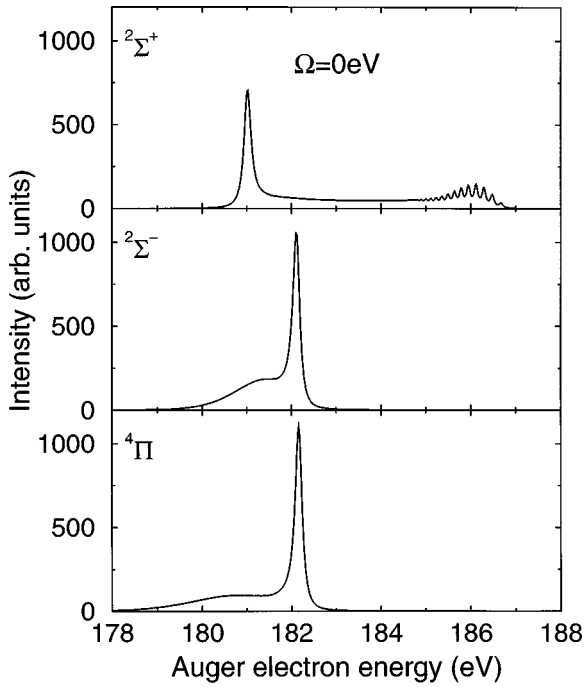

FIG. 5. RXS cross section of HCl for bound $^2\Sigma^+$ and dissociative $^2\Sigma^-$ and $^4\Pi$ final states. The case of monochromatic, resonant excitation ($\Omega=0$ eV).

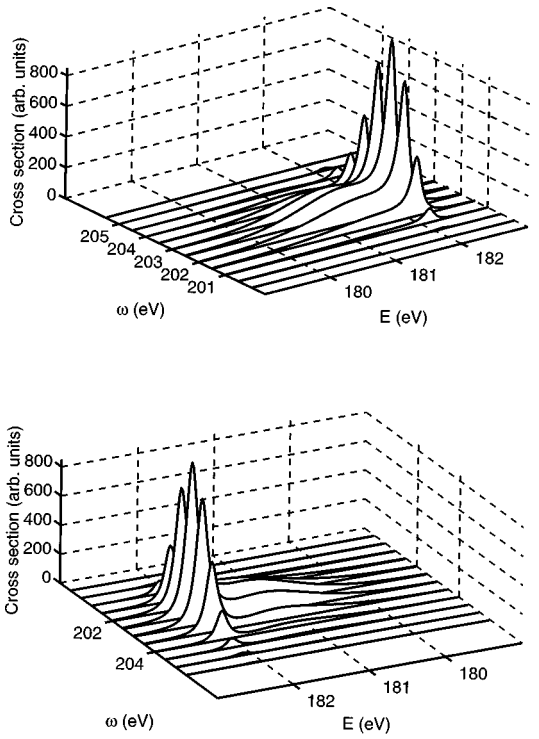

FIG. 6. RXS cross section for the nonbound $^2\Sigma^-$ final state of HCl for different excitation energies ω. The resonant frequency $[U_c(R_0)-E_0]$ of the vertical photoabsorption transition is equal to 202.58 eV. E is the energy of the Auger electron. One can see the fast decrease of the RXS cross section when the excitation energy is tuned out of the resonant frequency of the vertical photoabsorption transition. $\gamma=0$ eV.

final state can in general simultaneously have both blue and red tails [26,30]. It depends on the behavior of the potentials $U_c(R)$ and $U_f(R)$ close to the equilibrium geometry.

The spectral shape of the molecular tails strongly depends on the shape of $U_c(R)$ and $U_f(R)$. If the final (or core excited) state is bound the molecular contribution consists of a vibrational band and a smooth continuum-continuum tail (see upper panel in Fig. 5). Notice that the molecular contribution with the vibrational structure in this panel corresponds to the experimental band assigned in Ref. [27] as $5\sigma^{-1}$. The comparison with the experimental spectra [27] demonstrates that our simulations reproduce the main spectral features of the resonant Auger spectra of HCl.

The next question concerns the role of the detuning: As is well established now [26,15,18,27,29] the molecular and atomiclike contributions depend on the excitation energy in a qualitatively different manner. Indeed, the position of the atomiclike resonance does not depend on the excitation energy [26,25], while the center of gravity of the molecular band depends nonlinearly on Ω inside of the region of strong photoabsorption and follows a linear Raman law at the wings of the photoabsorption band [15]. Moreover, the weight of the atomiclike resonance tends to zero for large $|\Omega|$ faster than the molecular contribution. In this limit of sudden RXS only the molecular band contributes to the spectral shape of RXS. It is simply given by the FC factor between the ground and the final nuclear state [26,23] (see also Sec. VI B). All mentioned spectral features are shown in Figs. 6–9. The quenching of the RXS cross section when ω is

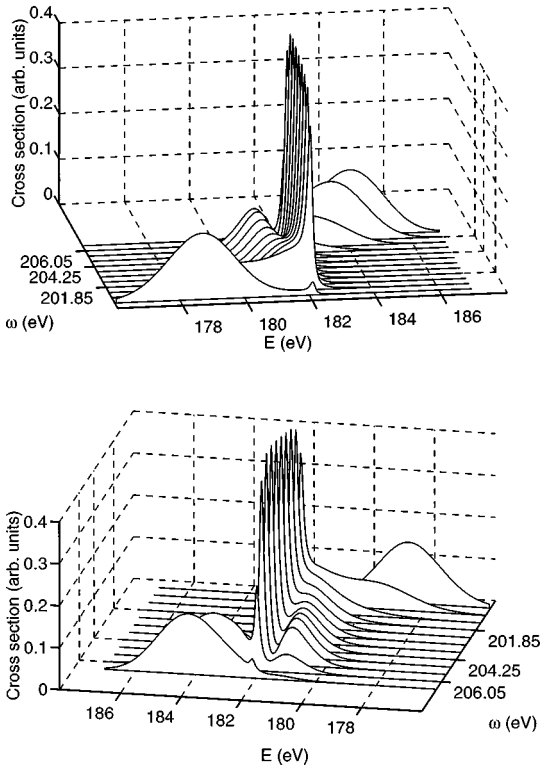

FIG. 7. RXS cross section for the nonbound $^2\Sigma^-$ final state of HCl for different excitation energies. The RXS cross sections are normalized; the integral cross sections are the same for different excitation energies. $\gamma=0$ eV.

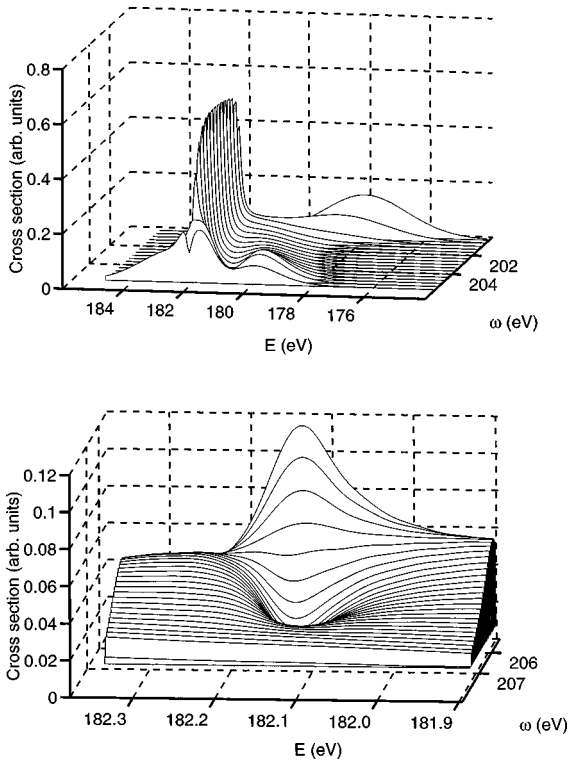

FIG. 8. RXS cross section for the unbound $^4\Pi$ final state of HCl for different excitation energies. The RXS cross sections are normalized; the integral cross sections are the same for different excitation energies. $\gamma=0$ eV. The lower panel shows in more detail the region near the spectral hole.

tuned below or above the photoabsorption band is shown in Fig. 10 in comparison with the spectral shape of photoabsorption. One can see that neither the RXS nor the absorption cross sections are symmetrical functions of the detuning. It is necessary also to emphasize that both these cross sections decrease slowly, more like Lorentzians than Gaussians (see also Sec. VI B). The switching over from Gaussian to Lorentzian behavior takes place for $E<200$ eV and is therefore not seen in the long-wave region (Fig. 10).

To focus attention only on the Ω dependence of the RXS spectral shape we depicted in Figs. 7–9 the RXS cross sections on the area of the corresponding spectral profiles. According to the reflection approximation (see Sec. V D) the RXS spectral profile maps the space distribution of the wave packet. This leads to the appearance of additional fine structure in the RXS profile [26,29] (Figs. 7 and 8) caused by the inhomogeneous space distribution of the core excited wave packet $|\Psi(0)\rangle$ in the molecular region (see Fig. 1, $\Omega=3$ eV, $R<3$ a.u.).

B. Interference between molecular and dissociative scattering channels

Figure 8 demonstrates the appearance of the additional spectral feature of the RXS profile when the narrow atomiclike resonance is embedded in the smooth molecular background. One can see that the atomiclike resonance converts into a spectral hole when ω is tuned from the photoabsorption resonance. This anomaly is the result of an interference between the molecular background and the atomiclike resonance channels. The possibility for such interference between resonant and off-resonant contributions was mentioned earlier [26]. Here we give a more extended explanation. We first note that the manifestation of this phenomenon is not the same as the Fano profile [35], although it reminds one thereof. For the sake of transparency we assume that both the core excited and the final states are dissociative and that the incident light beam is monochromatic. Then we get

$$\sigma(E,\omega)=|F|^2, \quad \epsilon_f=\omega+E_0-U_f(\infty)-E. \tag{43}$$

It is convenient to consider here the real core excited $|c\rangle=|\epsilon_c\rangle$ and final $|f\rangle=|\epsilon_f\rangle$ continuum nuclear states with the released dissociation energies ϵ_c and ϵ_f, respectively. Since the continuum-continuum Franck-Condon factor $\langle\epsilon_f|\epsilon_c\rangle$ is singular one can conclude that

$$\langle\epsilon_f|\epsilon_c\rangle\langle\epsilon_c|0\rangle=r(\epsilon_f,\Delta\epsilon_c)+s(\epsilon_c,\Delta\epsilon_c)\,\delta(\epsilon_f-\epsilon_c). \tag{44}$$

Here $\Delta\epsilon_c=\epsilon_c-\Delta U_c$ and $\Delta U_c=U_c(R_0)-U_c(\infty)$. The smooth function $s(\epsilon_c,\Delta\epsilon_c)$ shows the weight of the narrow atomiclike contribution while the smooth profile $r(\epsilon_f,\Delta\epsilon_c)$ is responsible for the molecular background [26,27]. Since the continuum wave functions are real functions, $s(\epsilon_c,\Delta\epsilon_c)$ and $r(\epsilon_f,\Delta\epsilon_c)$ are also real quantities. Equations (2) and (19), (44) infer that the scattering amplitude also is the sum of molecular and atomiclike contributions

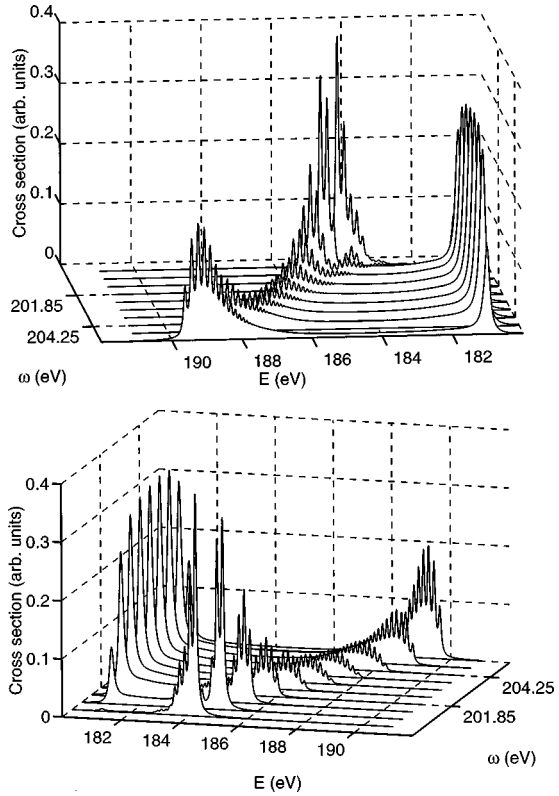

FIG. 9. RXS cross section for the bound $^2\Sigma^+$ final state of HCl for different excitation energies. The RXS cross sections are normalized; the integral cross sections are the same for different excitation energies. $\gamma=0$ eV.

$$F=\eta(\Omega,\Delta E)+\frac{s(\epsilon_f,\Omega)}{\Delta E+\imath\Gamma},$$

$$\eta(\Omega,\Delta E)=\eta_1(\Omega,\Delta E)+\imath\,\eta_2(\Omega,\Delta E), \tag{45}$$

$$s(\epsilon_f,\Omega)\propto\exp\left[-\frac{1}{2}\left(\frac{\Omega}{\gamma_c}\right)^2\right].$$

The essential point here is that the molecular contribution $\eta(\Omega,\Delta E)$ is now complex,

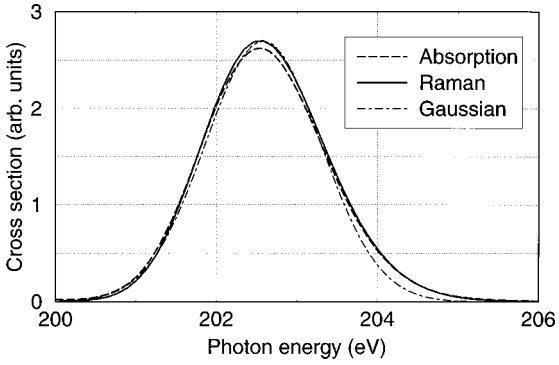

FIG. 10. Cross section of RXS integrated over E (solid line) and the Cl $2p$ x-ray photoabsorption (dashed line) in HCl. The core excited and final states are $2p^{-1}\sigma^*$ and $^2\Sigma^-$, respectively. The Gaussian profile is depicted as a dot-dashed line. Both cross sections have a maximum for $\omega\approx 202.58$ eV. The half-width at half maximum (HWHM) of the Gaussian is equal to 0.84 eV.

$$\eta_1(\Omega,\Delta E)=\int_{-\Delta U_c}^{\infty}d\Delta\,\epsilon_c\frac{(\Omega-\Delta\epsilon_c)b(\epsilon_f,\Delta\epsilon_c)}{(\Delta\epsilon_c-\Omega)^2+\Gamma^2},$$

$$\eta_2(\Omega,\Delta E)=-\int_{-\Delta U_c}^{\infty}d\Delta\,\epsilon_c\frac{\Gamma b(\epsilon_f,\Delta\epsilon_c)}{(\Delta\epsilon_c-\Omega)^2+\Gamma^2}, \tag{46}$$

as well as the atomiclike part. The interference between the molecular and the atomiclike contributions comes out naturally if the cross section (1) is written as the sum of direct and interference terms

$$\sigma(E,\omega)=\sigma_{\rm dir}(E,\omega)+\sigma_{\rm int}(E,\omega),$$

$$\sigma_{\rm dir}(E,\omega)=\sigma_{\rm dir}^{\rm mol}(E,\omega)+\sigma_{\rm dir}^{\rm at}(E,\omega). \tag{47}$$

The direct molecular and atomiclike contributions and interference term read

$$\sigma_{\rm dir}^{\rm mol}(E,\omega)=|\,\eta|^2,\quad \sigma_{\rm dir}^{\rm at}(E,\omega)=\frac{s^2}{\Delta E^2+\Gamma^2},$$

$$\sigma_{\rm int}(E,\omega)=\frac{2s(\Delta E\,\eta_1-\Gamma\,\eta_2)}{\Delta E^2+\Gamma^2}, \tag{48}$$

were $\eta_i\equiv\eta_i(\Omega,\Delta E)$, $s\equiv s(\epsilon_f,\Omega)$. One can observe a resemblance of the spectral shape of the atomiclike resonance with the well-known Fano profile [35] which describes the interference between continuum states and a discrete state embedded in this continuum. However, qualitative differences exist. In the case of interest the discrete state is missing both in the core excited and the final nuclear states. The reason for the appearance of the discrete resonance in the x-ray Raman spectrum is the cancellation of the kinetic energies in the resonant frequency of the decay transition, $U_c(\infty)+\epsilon_c-U_f(\infty)-\epsilon_f=U_c(\infty)-U_f(\infty)$, due to the effective conservation of the kinetic energy under decay in the dissociative region. This conservation relation is reflected by the singular part $\propto\delta(\epsilon_f-\epsilon_c)$ in the continuum-continuum overlap integral $\langle\epsilon_f|\epsilon_c\rangle$ (44).

Before proceeding to the analysis of the interference we discuss briefly the properties of the functions η_1 and η_2 which are responsible for the formation of the molecular band. Consider first the core excitation at the far wings of the photoabsorption band $\sqrt{\Omega+\Gamma^2}\gg\gamma_c$. In accordance with Eq. (45) the intensity of the narrow atomiclike resonance tends here exponentially to zero [26,27]. Its position does not depend on the excitation energy [26,25], Fig. 6. The molecular contribution also decreases, when $|\Omega|$ increases, but not so fast, only like a Lorentzian [26],

$$\eta_1\simeq\frac{\Omega}{\Omega^2+\Gamma^2}\langle f|0\rangle,\quad \eta_2\simeq-\frac{\Gamma}{\Omega^2+\Gamma^2}\langle f|0\rangle,$$

$$\langle f|0\rangle\propto\exp\left[-\frac{1}{2}\left(\frac{\Omega-\Delta E_0}{\gamma_f}\right)^2\right]. \tag{49}$$

Since the photoabsorption cross section is the imaginary part of the elastic RXS, apparently such a behavior (Lorentzian wings and a steep Gaussian-like resonant part) takes place also for photoexcitation to dissociative states. Equation (49) demonstrates the general phenomenon that the center of

gravity of the RXS profile follows the Raman law [15]: $\Delta E_0=\Omega$, where $\Delta E_0=E-[U_f(R_0)-U_f(R_0)]$ and $\gamma_f=a|U_f'(R_0)|$ is the width of the FC factor $\langle f|0\rangle$. η_1 and η_2 quench faster only when ω is tuned close to the photoabsorption band $\sqrt{\Omega+\Gamma^2}\lesssim\gamma_c$: $\eta_1\propto\eta_2\propto\langle\epsilon_c|0\rangle\propto\exp(-\Omega^2/2\gamma_c^2)$. The dispersion law in the photoabsorption region strongly differs from the Raman law [15]. The present numerical simulations also show this clearly, Figs. 7–9.

The limit of fast RXS is reached for quite large high $|\Omega|$. The simulations show that the RXS profile begins to copy the photoabsorption profile $|\langle f|0\rangle|^2$ (Figs. 7 and 8) of the $0\rightarrow f$ direct transition only when $\Omega\lesssim-3$ eV or when $\Omega\gtrsim4$ eV. As was shown in Sec. V D, the molecular contribution for moderate detunings has fine structure (Figs. 7,8) [26,29] caused by the inhomogeneous space distribution of the core excited state wave packet (Fig. 1). This fine structure disappears for very large detuning since in this asymptotic region the RXS cross section copies the profile of direct photoabsorption $0\rightarrow f$ (49). When the final state is bound ($^2\Sigma^+$ state) this photoabsorption profile has fine structure caused by the decay transitions to the vibrational levels of the final state (Fig. 9).

Apart from the evident asymmetry of the atomiclike profile, the interference leads to new striking spectral features: The first one is the total suppression of the atomiclike resonance if

$$\eta_1=0,\quad \eta_2=\frac{s}{2\Gamma}. \tag{50}$$

When $|\eta_1|\ll|\eta_2|$ (as in our simulations) and the weight of the molecular pedestal exceeds the amplitude s of the atomiclike part,

$$2\Gamma\,\eta_2 s>s^2, \tag{51}$$

an atomiclike ''hole'' emerges instead of the resonance peak (Fig. 8). This ''hole'' disappears for large detunings where the RXS profile coincides with the photoabsorption band (49) of the direct $0\rightarrow f$ transition (see lower panel in Fig. 8).

A naive picture prompts that any narrow spectral feature is blurred when the spectral width γ of the incident radiation increases. The computations show something different, however, see Fig. 11. Indeed, one can see that the width of the spectral hole as well as that of the atomiclike band is practically independent of γ [26,25]. Moreover, Fig. 11 demonstrates another unexpected effect, namely, the transformation of the hole into a peak when γ increases. This atomiclike feature can be understood if one recalls that broadband excitation implies a summation of the RXS cross sections for different ω. If the particular ω with the sharp peak, Fig. 8, is included in the summation, then it might dominate for large γ and there will be a peak instead of as a hole.

Figure 10 shows simulations of the asymmetry of the RXS profile as a function of Ω [$\eta(\Omega,\Delta E)\neq\eta(-\Omega,\Delta E)$]. One reason for the asymmetry is the finite value of ΔU_c in Eq. (46). In general, this asymmetry is caused by the inhomogeneous density of core excited states.

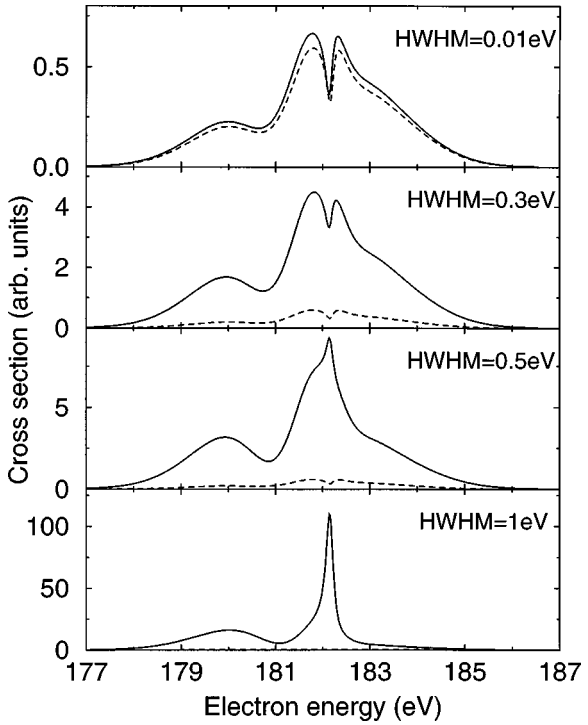

FIG. 11. Spectral profile vs spectral width γ of incident radiation. The final state is $^4\Pi$ (see Fig. 8). The RXS cross sections are normalized. The spectral function is approximated by a Gaussian (6) with the pilot frequency 206 eV and the following values of HWHM: $\gamma\sqrt{\ln 2}=0.01$, 0.3, 0.5, 1 eV. The RXS cross section for monochromatic excitation is depicted by a dashed line.

VII. SUMMARY

In the present paper three qualitatively different time-dependent wave-packet formalisms for radiative and nonradiative x-ray Raman scattering were presented and compared. The first one, a ''two-step'' method, is based on two coupled Schrödinger equations describing the dynamics in the core excited and final states, respectively. The second, a ''one-step'' approach, requires the solution of only one time-dependent Schrödinger equation, but with the effective time-dependent Hamiltonian depending on the potentials of both the core excited and the final states. In the problems concerning only nuclear dynamics this Hamiltonian reduces in the interaction representation to the simple difference of the potentials of the core excited and final states. The third method is based on the convolution of the spectral function of the incident radiation with the RXS cross section for the monochromatic incident light beam. This approach requires the solution of only a single Schrödinger equation. We used the latter time-dependent formalism to calculate the resonant Auger electron decay spectra of the HCl molecule for the $2p^{-1}\sigma^*$ core excited and three different final states; the bound $^2\Sigma^+$ and the dissociative $^2\Sigma^-$ and $^4\Pi$ states, having all potential surfaces computed *ab initio*. Our simulations demonstrate the strong dependence of the spectral profile on the excitation energy—that is, on the RXS duration time. We demonstrate that the RXS profile of HCl consists of a narrow atomiclike peak and a broad molecular background (far wing) with fine structure that agrees with previous results [26,27]. We have shown that the center of gravity of the molecular background follows approximately the Raman law

when the excitation energy is tuned out of the photoabsorption band, while the position of the atomiclike resonance does not depend on the excitation energy. When the excitation energy is tuned inside the photoabsorption band the dispersion law for the center of gravity of the molecular pedestal shows non-Raman behavior [15]. According to previous results [26,27] the ratio of the atomiclike spectral feature to the molecular background strongly depends on the RXS duration. The atomiclike resonance is suppressed, up to depletion, for fast RXS corresponding to the excitation energies tuned out of the photoabsorption band.

We predict an effect of a total quenching of the atomiclike resonance for certain excitation energies. Moreover, when the excitation energy continues to change, the atomiclike resonance turns into a narrow spectral hole. The physical origin of these new phenomena is given by the interference between the molecular background and the atomiclike channels. We have also found a corresponding transformation of this spectral hole into an atomiclike resonance when the spectral width of incident radiation increases.

We have shown that the spectral profile of the atomiclike resonance is formed by a central Lorentzian part with blueshifted or redshifted near wings. These near wings are caused by the long-range part of the interatomic potentials. A method was suggested based on the ''spectroscopy of the wings'' of the atomiclike resonance, by which the long-range part of the potentials is mapped.

The present theory shows that the RXS cross section is proportional to the square wave packet of the core excited state and copies in a certain sense its space distribution, something that allows a mapping of the square of this wave packet.

ACKNOWLEDGMENTS

The present project has been generously supported by NSC, the Swedish National Supercomputer Center in Linköping, and by the Swedish Natural Science Research Council.

APPENDIX A: WIGNER'S TRANSFORM

We recapitulate here some basic results from the theory of the Wigner transform concerning the Franck-Condon problem (see papers [36,37], and references therein). The first results refer to the fact that the trace of the Wigner transform (24) of the product of two operators is equal to the product of the two Wigner transforms. The application of this fact to Eq. (23) yields

$$\sigma(E,\omega)=\frac{1}{2\pi\hbar}\int dp\,dR\,\delta(\mathcal{E}-H_f)_w(p,R)\rho_w(p,R). \tag{A1}$$

Then we need also the expansion

$$\delta(\mathcal{E}-H_f)_w(p,R) = \left[1-\hbar^2\left(f_2\frac{\partial^2}{\partial\mathcal{E}^2}-f_3\frac{\partial^3}{\partial\mathcal{E}^3}\right)\right]\delta(\mathcal{E}-H_f(p,R))+0(\hbar^4), \tag{A2}$$

where $H_f(p,R)=p^2/2\mu+U_f(R)$ is the classical Hamilton function, $f_0=1$, $f_2=U_f''(R)/(8\mu)$, $f_3=U_f'^2/(24\mu)+p^2U_f''(R)/(24\mu^2)$. This equation results in the following expansion of the RXS cross section:

$$\sigma(E,\omega)=\sigma^{(0)}(E,\omega)-\hbar^2 \times\left(\frac{\partial^2}{\partial\mathcal{E}^2}\sigma^{(2)}(E,\omega)-\frac{\partial^3}{\partial\mathcal{E}^3}\sigma^{(3)}(E,\omega)\right)+\cdots,$$

$$\sigma^{(i)}(E,\omega)=\frac{1}{2\pi\hbar}\int dp\,dR\,\delta(\mathcal{E}-H_f)_w(p,R)\rho_w(p,R)f_i. \tag{A3}$$

If the Hamiltonian H_f is replaced by the classical Hamilton function $H_f(p,R)$, the first term, $\delta(\mathcal{E}-H_f(p,R))$, in the $\hbar$ expansion for the density of states $\delta(\mathcal{E}-H_f)_w(p,R)$ is obtained, and so we may write the semiclassical version (25) of Eq. (A1). One needs also the following connection between the diagonal element of the density matrix ρ in the R and p representations and the Wigner function ρ_w:

$$\rho(R,R)=\frac{1}{2\pi\hbar}\int dp\,\rho_w(p,R),\quad \rho(p,p)=\int dR\,\rho_w(p,R). \tag{A4}$$

APPENDIX B: SPACE DISTRIBUTION OF STATIONARY WAVE PACKETS

In this appendix the space properties of the wave packet $\Psi(R,0)$ (17), (22) are outlined. To be specific we restrict the present analysis to the case $D=\text{const}$, $Q=\text{const}$ (19). We begin with the representation of the wave packet (22),

$$\Psi(R,0)=\langle R|\Psi(0)\rangle=\langle R|G|0\rangle=G|0\rangle \simeq i\int_{R_0}^{R_d}dR'\,G(R,R')\varphi_0(R') \tag{B1}$$

in the terms of the lifetime-broadened Green function

$$G(R,R')=\int d\epsilon_c\frac{\langle R|\epsilon_c\rangle\langle\epsilon_c|R'\rangle}{\mathcal{E}_0-E_c+i\Gamma}, \tag{B2}$$

where $\mathcal{E}_0=\omega+E_0$ and $E_c=\epsilon_c+U_c(\infty)$ is the eigenvalue of H_c. The continuum nuclear wave function can be written in the semiclassical approximation as

$$\langle R|\epsilon_c\rangle=\frac{A}{\sqrt{p(R)}}\exp\left(-\imath\int_{R_0}^{R}p(R')dR'\right), \tag{B3}$$

with momentum $p(R)=[2\mu(E_c-U_c(R)]^{1/2}$ and A as the normalization constant. Insertion of this into Eq. (B2) shows that the lifetime-broadened Green function is defined by the product [26]

$$G(R,R')\simeq G_0(R,R')e^{-\Gamma\tau_f(R,R')},\quad \tau_f(R,R')=\int_{R'}^{R}\frac{dR''}{v(R'')} \tag{B4}$$

of the ordinary Green function G_0 (with $\Gamma=0$),

$$G_0(R,R')\simeq -\frac{2\pi\imath|A|^2}{\sqrt{p(R)p(R')}}\exp\left(\imath\int_{R'}^{R}p(R'')dR''\right) \tag{B5}$$

and the factor $\exp[-\Gamma\tau_f(R,R')]$ which is responsible for the damping of the emission rate due to the finite lifetime of the core excited state. Here $E_c=\mathcal{E}_0$.

[1] T. Åberg and B. Crasemann, in *Resonant Anomalous X-Ray Scattering. Theory and Applications*, edited by G. Materlik, C. J. Sparks, and K. Fischer (North-Holland, Amsterdam, 1994), p. 431.

[2] P. L. Cowan, in *Resonant Anomalous X-Ray Scattering. Theory and Applications*, edited by G. Materlik, C. J. Sparks, and K. Fischer (North-Holland, Amsterdam, 1994), p. 449.

[3] W. Eberhardt, in *Applications of Synchrotron Radiation*, edited by W. Eberhardt, Springer Series in Surface Sciences Vol. 35 (Springer-Verlag, Berlin, 1995), p. 203.

[4] N. Mårtensson, in *Applications of Synchrotron Radiation* (Ref. [3]), p. 65.

[5] J. Nordgren, J. Phys. (France) IV **7**, C2-9 (1997).

[6] S. Svensson and A. Ausmees, Appl. Phys. A: Mater. Sci. Process. **65**, 107 (1997).

[7] K. Ueda, H. Chiba, Y. Sato, T. Hayaishi, E. Shigemasa, and A. Yagishita, J. Chem. Phys. **101**, 3520 (1994).

[8] M. Simon, C. Miron, N. Leclercq, P. Morin, K. Ueda, Y. Sato, S. Tanaka, and Y. Kayanuma, Phys. Rev. Lett. **79**, 3857 (1997).

[9] K. Siegbahn, C. Nordling, G. Johansson, J. Hedman, P. F. Hedén, K. Hamrin, U. Gelius, T. Bergmark, L. O. Werme, R. Manne, and Y. Baer, *ESCA Applied to Free Molecules* (North-Holland, Amsterdam, 1969).

[10] L. O. Werme, B. Grenberg, J. Nordgren, C. Nordling, and K. Siegbahn, Nature (London) **242**, 453 (1973).

[11] F. Kh. Gel'mukhanov, L. N. Mazalov, and A. V. Kondratenko, Chem. Phys. Lett. **46**, 133 (1977).

[12] P. Skytt, P. Glans, K. Gunnelin, J. Guo, and J. Nordgren, Phys. Rev. A **55**, 146 (1997).

[13] R. Fink, J. Chem. Phys. **106**, 4038 (1997).

[14] M. N. Piancastelli, M. Neeb, A. Kivimäki, B. Kempgens, H. M. Köppe, K. Maier, A. M. Bradshaw, and R. F. Fink, J. Phys. B **30**, 5677 (1997).

[15] F. Gel'mukhanov and H. Ågren, Phys. Rev. A **54**, 3960 (1996).

[16] R. Colle and S. Simonucci, Mol. Phys. **92**, 409 (1997).

[17] R. Colle and S. Simonucci, Nuovo Cimento D **20**, 29 (1998).

[18] F. Gel'mukhanov, T. Privalov, and H. Ågren, Phys. Rev. A **56**, 256 (1997).

[19] S. Sundin, F. Gel'mukhanov, H. Ågren, S. J. Osborne, A. Kikas, O. Björneholm, A. Ausmees, and S. Svensson, Phys. Rev. Lett. **79**, 1451 (1997).

[20] Y. Ma, P. Skytt, N. Wassdahl, P. Glans, D. C. Mancini, J. H. Guo, and J. Nordgren, Phys. Rev. Lett. **71**, 3725 (1993).

[21] L. S. Cederbaum, J. Chem. Phys. **103**, 562 (1995).

[22] P. Skytt, P. Glans, J.-H. Guo, K. Gunnelin, J. Nordgren, F. Gel'mukhanov, A. Cesar, and H. Ågren, Phys. Rev. Lett. **77**, 5035 (1996).

[23] A. Cesar, F. Gel'mukhanov, Y. Luo, H. Ågren, P. Skytt, P. Glans, J.-H. Guo, K. Gunnelin, and J. Nordgren, J. Chem. Phys. **106**, 3439 (1997).

[24] Z. F. Liu, G. M. Bancroft, K. H. Tan, and M. Schachter, Phys. Rev. Lett. **72**, 621 (1994).

[25] E. Kukk, H. Aksela, S. Aksela, F. Gel'mukhanov, H. Ågren, and S. Svensson, Phys. Rev. Lett. **76**, 3100 (1996).

[26] F. Gel'mukhanov and H. Ågren, Phys. Rev. A **54**, 379 (1996).

[27] O. Björneholm, S. Sundin, S. Svensson, R. R. T. Marinho, A. Naves de Brito, F. Gel'mukhanov, and H. Ågren, Phys. Rev. Lett. **79**, 3150 (1997).

[28] E. Pahl, H.-D. Meyer, and L. S. Cederbaum, Z. Phys. D **38**, 215 (1996).

[29] E. Pahl, L. S. Cederbaum, H.-D. Meyer, and F. Tarantelli, Phys. Rev. Lett. **80**, 1865 (1998).

[30] F. Gel'mukhanov, H. Ågren, and P. Sałek, Phys. Rev. A **57**, 2511 (1998).

[31] F. Gel'mukhanov and H. Ågren, Phys. Rev. A **49**, 4378 (1994).

[32] T.-Y. Wu and T. Ohmura, *Quantum Theory of Scattering* (Prentice-Hall, New York, 1962).

[33] H. Ågren, A. Cesar, and V. Carravetta, Chem. Phys. Lett. **139**, 145 (1987).

[34] T. Helgaker, H. J. Aa. Jensen, P. Jørgensen, J. Olsen, K. Ruud, H. Ågren, T. Andersen, K. L. Bak, V. Bakken, O. Christiansen, P. Dahle, E. K. Dalskov, T. Enevoldsen, H. Heiberg, H. Hettema, D. Jonsson, S. Kirpekar, R. Kobayashi, H. Koch, K. V. Mikkelsen, P. Norman, M. J. Packer, T. Saue, P. R. Taylor, and O. Vahtras, Dalton, an *ab initio* electronic structure program, Release 1.0 (1997). See http://www.kjemi.uio.no/software/dalton/dalton.html.

[35] U. Fano, Phys. Rev. **124**, 1866 (1961).

[36] E. J. Heller, J. Chem. Phys. **68**, 2066 (1978).

[37] B. Hüpper and B. Eckhardt, Phys. Rev. A **57**, 1636 (1998).